Maximum Interconnectedness and Availability for Directional Airborne Range Extension Networks

Thomas Shake, *Senior Member, IEEE*, Rahul Amin, *Member, IEEE*

Abstract

Extending the range of tactical military networks that are confined to a local geographic area by using small aircraft to relay traffic to geographically distant areas is a topic of interest in military network technology development. Highly directional antennas, incorporated into avionics pods that attach modularly to an aircraft fuselage, can provide long-range, interference-resistant communications at high data rates for range extension. Antenna elements in such designs typically have limited field-of-view (FoV), potentially making interconnectedness among communication nodes dependent on the geometry of the physical network. This paper examines generic sectorized and non-sectorized pod antenna designs and compares the interconnectedness and link availability of these designs in representative range extension network layouts. Mathematical criteria for 100% link availability are presented, and quantitative trade-offs between link availability and node interconnectedness are derived as functions of the number of antenna beams per pod, the number of beams per sector, and the number of surface users to be supported.[1]

Index Terms

Range extension, directional networks, network topology, beamforming.

Thomas Shake and Rahul Amin are with the Tactical Networks Group at MIT Lincoln Laboratory, Lexington, MA 02420 USA e-mail: (shake@ll.mit.edu, rahul.amin@ll.mit.edu)

[1]Distribution A: approved for public release; unlimited distributon. This work is sponsored by the United States Department of the Navy under Air Force Contract #FA8721-05-C-0002. Opinions, interpretations, recommendations and conclusions are those of the authors and are not necessarily endorsed by the United States Government.

I. Introduction

Tactical military networks both on land and at sea often have restricted transmission ranges due to limits on terminal transmission power, geographic features that block line-of-sight, and poor over-the-horizon signal propagation. Limiting communications to local tactical areas can strongly constrain mission success, and some form of range extension is often needed for these tactical networks. One frequently considered option for range extension is the use of relatively small unmanned aircraft to serve as over-the-horizon relay platforms connecting geographically separated local groups of surface nodes. Fig. 1 shows a conceptual example of such a range-extension scenario that includes both maritime and land-based communication terminals.

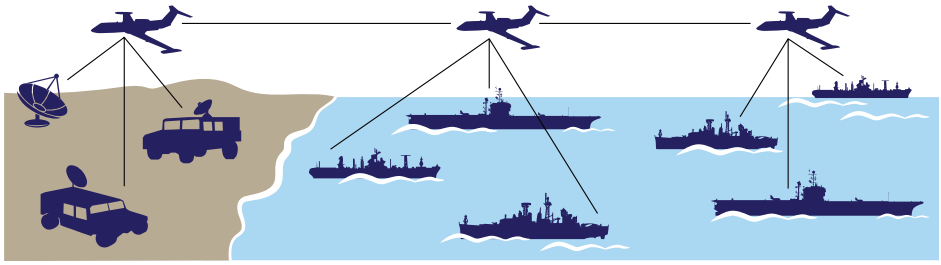

Fig. 1. Conceptual example of network range extension via aerial platforms

A promising method of incorporating electronics and antennas into an airborne relay platform is to enclose them in a separate pod, which can be modularly designed and attached to the bottom of the wings or fuselage of a variety of aircraft types [1]. Fig. 2 shows a generic concept for such a pod design with potential antenna placements on the ends, sides, and bottom of the pod. There is great advantage to making these antennas highly directional; this enables both a much higher data rate connection between aircraft and a higher level of rejection of local interference in both surface-to-air and air-to-air connections. Such directional antennas may be implemented by mechanically steered dish antennas or by electronically steered devices (e.g., phased arrays). However, using highly directional antennas also makes the design, discovery, and maintenance of the relay network topology significantly more difficult.

Depending on which of the potential antenna placements shown in Fig. 2 is used for a given design, the line-of-sight (LOS) between two aircraft or between aircraft and surface nodes may undergo intermittent blockages as the aircraft fly in patterns that enable them to maintain LOS to a local surface node group. (The flightpaths typically considered for such range extension

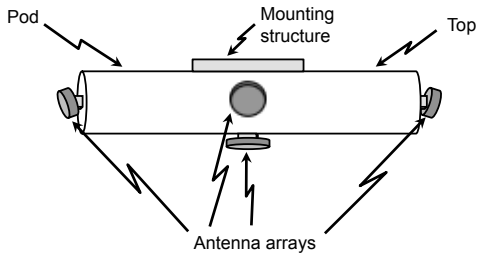

Fig. 2. Generic pod concept for modular aerial electronics

purposes are closed paths with circular or racetrack-shaped patterns [1].) Antennas placed on the ends and sides of the pod are especially vulnerable to regular blockages, and such blockages are an important factor affecting the design and management of the network topology [2][3]. In particular, such blockages can cause significant periods of unavailability of the range extension capability as seen by surface nodes in local groups. While antenna placement on the bottom of a pod has significant advantages for maintaining visibility to surface nodes with minimal blockage, this pod location may sometimes be needed for other components such as sensor arrays or secondary communication antennas.

In addition to the multiple options for locating antenna arrays or elements on the pod, there are also multiple types of antenna designs that can be considered. One design could be to place multiple mechanically steered dish antennas on various parts of the pod [1]. Alternatively, electronically steered arrays of multiple fixed antenna elements may be used. Such arrays may be designed in a sectorized system [4][5], where antenna beams in each sector are formed independently from those in other sectors. They may also be designed in non-sectorized system where a centralized beamformer takes inputs from all the elements on the pod and forms beams in various directions [6][7]. The design trades among these various options are mostly beyond the scope of this paper, but since practical considerations may cause a particular design to use any of the options described above, this paper quantifies several key performance parameters in ways that cover all of these options.

This paper derives mathematical relationships and algorithms that quantify trade-offs among several parameters, including 1) the degree of interconnectedness[2] that can be attained among

[2]We use the term *interconnectedness* (defined quantitatively in Section IV-A) to distinguish the specific parameter we consider from *connectivity*, which has a standard definition in graph theoretic and networking literature that is related to, but different from, the metric we consider.

communication nodes in separated local groups; 2) the availability of the links between local users and relay aircraft; 3) the number of surface nodes per aircraft that can be supported; and 4) the number of directional antenna beams that can be incorporated into a given pod design.

The outline of the rest of the paper is as follows: Section II surveys previous work in this area. Section III describes the range extension network model and design parameters. Section IV develops quantitative relationships among key design elements and performance metrics. Section V considers some implications of the results in Section IV for range extension network topology design and for technology development. Section VI summarizes the results and offers some concluding thoughts.

II. Previous Work

Various aspects of the performance of wireless networks using highly directional antennas have been addressed in the literature. There is a significant body of work on Medium Access Control (MAC) for wireless ad hoc networks with directional antennas, which is surveyed in [9]. This work generally focuses on the problems of MAC layer protocols specific to directional systems, such as *deafness*, *blocking*, and certain *hidden terminal* issues unique to directional systems. Topology management for wireless ad hoc and sensor networks has also received extensive attention, and is surveyed in [8]. Most of this work assumes either static nodes, omni-directional transmissions, or both, and has limited applicability to systems with highly directional transmission. Free-space optical topologies, which must deal with inherently highly directional transmission, are considered in several works. References [12] and [13] propose topology control heuristics based on minimizing bit-error-rate and network congestion, and show improvements in network performance measures such as latency, congestion, and dropped packets. Improvements in network throughput performance are obtained by a heuristic integrating network routing and physical interface constraints in [14]. The above works do not directly address maximizing network link and path availability or connectivity, and do not model the effects of the intermittent nature of aerial links with periodic field-of-view blockages.

Several papers have specifically modeled aerial and maritime military networks with directional antennas. Aerial network topology management heuristics have been proposed in [10], which compares performance metrics such as total delivered data, network betweenness centrality, all-terminal reliability of three different heuristics and shows a trade-off between performance and computational requirements for a genetic algorithm-based topology management heuristic.

Reference [11] models range extension networks using directional antennas and optimizes the choice of antennas with multiple aerial nodes and multiple antennas per node. At-sea demonstrations of a ship-based directional networking system are presented in [5]. This work included demonstration of successful ship-to-ship transmission and tracking with directional antennas and multiple radio-per-node architecture. None of the above work, as far as the authors are aware, focuses on overall network connectivity or link or path availability, or models links with periodic field-of-view blockages due to structural factors such as aircraft fuselage or pod structures.

Graph theoretic approaches to characterizing connectivity and survivability have been extensively researched (see [20][23][24] for example), and network reliability theory also applies to issues of connectivity and availability [21]. However, the topologies characteristic of range extension networks have not received significant attention and intermittent field-of-view blockages have not been considered. The issue of pod-based antenna blockage has been addressed in [1][2][3]. The first of these papers examines the effects of platform dynamics and aircraft orbit shapes on connection availability, but does not generalize the analysis to arbitrary topologies or consider more than two antennas per pod. The second and third of these papers concentrate on the effects of antenna switching on specific small-scale scenarios. The current paper models pod-based antenna blockages in a way that allows generalization to arbitrary topologies with arbitrary numbers of aircraft and surface nodes, and presents new closed-form analytical results for low-degree air topologies. A previous paper calculated interconnectedness and availability results for a specific two-sector design with no field-of-view overlap between the sectors and considered the implications for network topology management [15]. The current paper extends these results to an arbitrary number of sectors with arbitrary degrees of overlap in field-of-view, and also adds a quantitative evaluation of the quality of modeling approximations.

III. Range Extension Network Model

A. System Model

This paper quantifies the effects of antenna field-of-view (FoV) on both the interconnectedness of surface nodes in multiple network enclaves and the availability of the aerial relay communication links. This section describes our system model, which is summarized in Table I.

There are N aircraft nodes serving as range extension relays, with S^i surface nodes in communication range of aircraft i, $1 \leq i \leq N$. Each aircraft has an electronics pod providing

TABLE I

SYSTEM MODEL PARAMETERS

Modeling Parameters			
N	# of aircraft nodes	γ	Angular overlap in azimuth between antenna sectors
S^i	# of surface nodes under air node i	δ	Angular overlap in elevation between antenna sectors
n_a	# of total antenna beams per aircraft	σ	Angular field-of-view (FoV) of each antenna sector
n_s	# of antenna sectors per aircraft	β^i_j	Azimuth at air node i of air node j
d^i_{air}	# of air nodes connected to node i	T^i	Time for aircraft i to fly one complete orbit
Performance Metrics			
K	Total number of surface nodes that can be connected to the air backbone		
A_f	Fractional availability of surface-to-air links		

a total of n_a highly directional antenna beams, which are divided evenly among n_s sectors as shown in Fig. 3. The sectors have angular FoV of σ^o and an azimuthal overlap with each adjacent sector of γ^o. The n_a/n_s antenna beams in each sector can be pointed in any direction within the sector's FoV. Note that setting $n_s = 1$ models a non-sectorized design where n_a beams can be pointed in any azimuthal direction without restriction. We assume that antenna elements/arrays on the pod sides or ends would be designed to have an elevation FoV that extends at least 90^o from aircraft nadir up to $10 - 20^o$ above horizontal. Mechanically steered antennas could easily be gimbaled to accomplish this range of motion, and phased arrays could be designed to accommodate this range angular FoV in elevation.

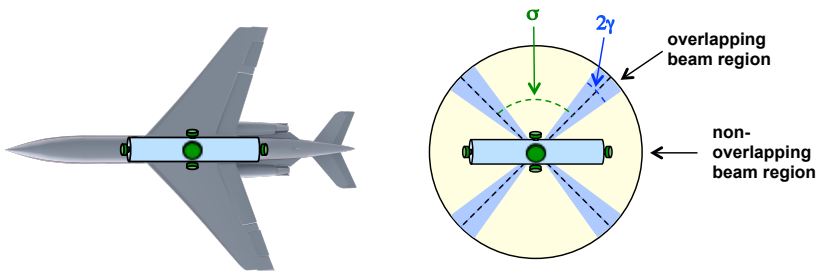

Fig. 3. Generic pod antenna model

Each aircraft flies in a closed, near-circular flightpath, which repeats every T^i seconds, and is connected to d^i_{air} other air nodes. We assume that d^i_{air} remains constant in this paper, though

many of the results can be generalized to allow it to vary with time.[3] The azimuth angles (at node i) of these d^i_{air} nodes are denoted by β^i_j as illustrated in Fig. 4. The aircraft are assumed to be relatively far away from each other (otherwise the range extension provided would be poor) and the radii of their flightpaths are assumed to be small compared to the distance between the aircraft. A representative node layout is illustrated in Fig. 5, with possible two low-degree air topologies overlaid. This figure shows the centroids of racetrack flightpaths as light circles; the realistically modeled racetrack flightpaths are the thin lines around the centroids. The surface nodes are shown with linear paths, and the light triangles represent specific positions of the nodes at a particular point in time. Solid white lines represent the air-to-air connections, and dashed lines show air-to-surface connections.

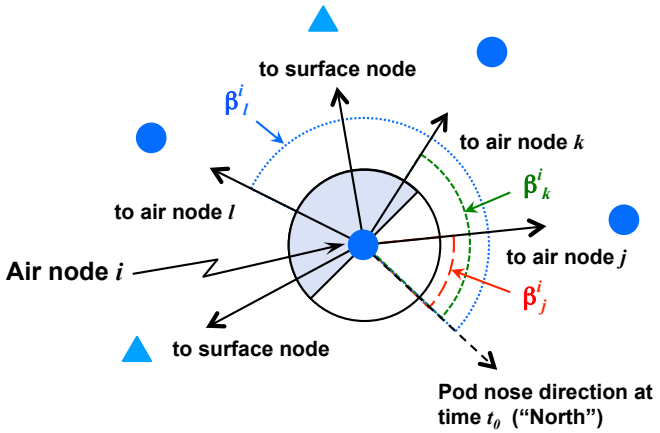

Fig. 4. Azimuth plane view of air node i

An important modeling choice is how to handle antenna elements that may be placed on the bottom of the pod. Bottom-mounted elements or arrays will tend to have clear visibility of local nodes on the earth's surface but may have poorer visibility (e.g., longer periods of line-of-sight blockage) of other aircraft nodes. A logical choice for pod antenna designs would be to place antenna elements/arrays for local node connectivity on the bottom of the pod and to use the sides and/or ends of the pod for antennas intended to connect to other aerial nodes. However, there are important scenarios where this type of design may be precluded, such as when the bottom of the pod must be reserved for sensor arrays or other equipment. We therefore choose to focus on the azimuthal model above where the bottom of the pod is not available for communication antennas

[3]This assumption implies that the air topology is designed so that d^i_{air} nodes can be supported at all times by the antenna design. See [15] for discussion of some pertinent air topology considerations.

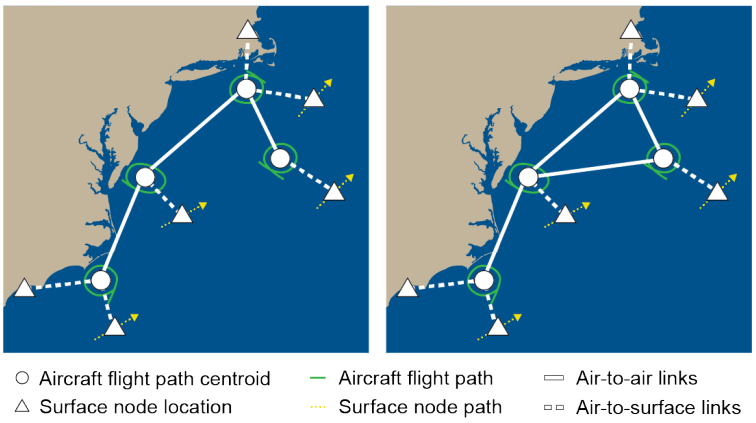

Fig. 5. Representative practical range extension network topologies

to be used for range extension. We note that the interconnectedness and availability results for a design using the bottom of the pod for local communication antennas would resemble those for the model above with $n_s = 1$ sector, which are included in the analysis of this paper. The rest of the paper will focus on the azimuthal model in Fig. 3 and will assume that the bottom of the pod is not used for range extension antenna elements.

B. Key Modeling Approximations

The interconnectedness and availability modeling in this paper is based on two key approximations:

1) Compass directions from a given air node to other nodes are assumed to be approximately constant as the aircraft moves.
2) Antenna Field-of-View (FoV) blockages are modeled by fixed azimuth and elevation limits.

These approximations enable a general mathematical analysis of an otherwise specific and complicated situation. The first approximation is that the relative compass direction of both air and surface nodes as seen from any air node changes only negligibly during the time it takes to complete one circuit of the closed flightpath. This should be approximately true for other air nodes for most practical range extension scenarios. It should also be approximately true for many surface node distributions, but may not be such a good approximation for scenarios where the surface nodes are located close to the air relay node. However, Appendix B will show that this approximation produces little or no error in the performance metrics modeled in this paper for circular flight paths as long as they are averaged over an integer number of circuits of the flight path.

The second key approximation is in how antenna FoV on each pod is modeled. In the sectorized azimuthal model of Fig. 3, the FoV boundaries of each sector may be defined by pod structure blockage, gimbal restrictions, or array off-axis pointing limitations for designs with $n_s > 1$. Both azimuth and elevation angle FoV boundaries are most likely to be due to structural blockages (pod body, aircraft fuselage or wings). While the geometry of FoV blockages is likely to vary with individual aircraft and pod designs, a generic model of fixed azimuth and elevation boundaries is a reasonable approximation for analytical purposes. An example of boundaries for a 2-sector design with antennas mounted on the pod ends is shown in Fig. 6a.

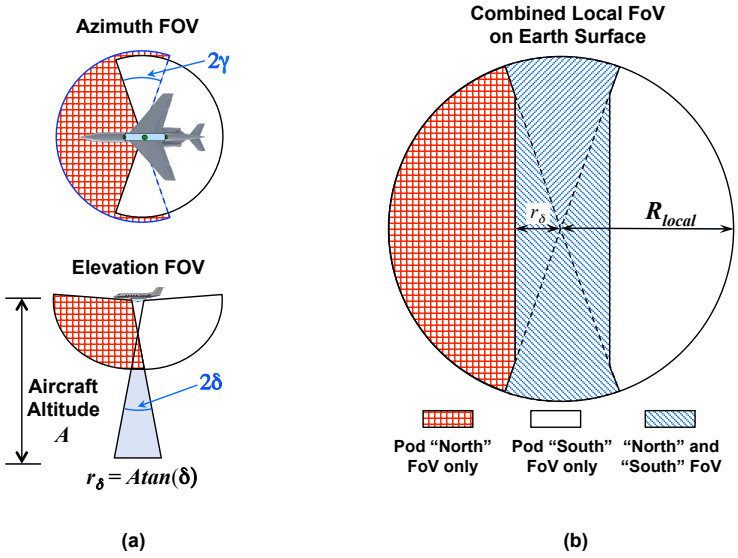

Fig. 6. Two-sector FoV example: (a) fixed FoV limits, (b) coverage areas on the surface of the earth

With these approximations, the visibility of both air and surface nodes from air node i can be determined solely from the knowledge of the node's azimuth, β_j^i, for air nodes, and by the combination of the node's azimuth and its distance from the nadir of aircraft i for surface nodes. Since air node i's flight path is approximated by a circle of essentially zero radius, as the aircraft flies around one circuit of its path the directions to the other nodes simply rotate in the azimuth plane of air node i.

IV. Interconnectedness and Availability Maximization

A. Evaluation Criteria

We define the *interconnectedness* of the surface nodes as the total number of end-to-end communication paths that may be formed between different surface nodes. For our range ex-

tension scenario, this is equal to the total number of unordered pairs of surface nodes (a, b) between which communication paths exist. (Note that this notion of interconnectedness differs from the standard graph theoretic notion of the *connectivity* of a graph [19][20].) This models an important aspect of the ability of a range extension network to enable the exchange of data among a maximum number of geographically distributed users. Assuming that the air backbone is connected in the standard graph theoretic sense, maximizing the total number of surface-to-air connections in the network is equivalent to maximizing interconnectedness. Hence, this paper focuses on maximizing 1) the total number of surface nodes that can be connected to the air backbone (and therefore to each other), denoted here by K, and 2) the fractional availability of each of these connections, denoted here by A_f, where availability is defined in the usual way as $Uptime/[Uptime + Downtime]$ over any given period of time [22]. Both of these maximizations are functions of antenna design and FoV parameters n_a, n_s, γ, δ, and of topology parameters β^i_j, S^i, N, and T^i.

The number and availability of interconnections among surface nodes are relatively simple quantities to model, have great importance in practical military range extension scenarios, and can be expressed as functions of the design variables just mentioned. Other network design optimizations were considered, and have been reported in the research literature, most notably maximizing some form of all-to-all traffic subject to topology restrictions (see, for example, [10][16]). This type of optimization is complex and involves multi-commodity flow optimization [17] and fairness issues [18], and is difficult to measure and evaluate in realistic network scenarios. Furthermore, many range extension scenarios do not allow prediction of the traffic characteristics or requirements, making it difficult to match the optimization to the realistic network requirements.

The specific performance measures of interconnectedness and availability considered here are:

- The average number of surface nodes that can be connected to the air backbone, $\langle K \rangle$
- The average fractional availability of surface-to-air connections, $\langle A_f \rangle$

where the notation $\langle x \rangle$ refers to the expected value of x, and where $\langle A_f \rangle$ is given by

$$\langle A_f \rangle = \frac{\langle K \rangle}{\sum_{i=1}^{N} S^i} \tag{1}$$

and may be apportioned either evenly or unevenly among surface nodes.

B. General results

Reference [15] gives an upper bound on K/N, the total number of connectable surface nodes per aircraft, for the specific case of $n_s = 2$ sectors and $\gamma = \delta = 0^o$ (i.e., no antenna FoV overlap in either azimuth or elevation) and $S^i = S^j \ \forall i, j$. This upper bound holds when these restrictions are removed, and with minor modifications to adjust to the notation in the current paper it becomes:

$$\frac{K}{N}^U = \frac{1}{N}\sum_{i=1}^{N}(n_a - d^i_{air}) \tag{2}$$

This is a straightforward consequence of the fact that antenna beams that are used for the air topology are not available to be used to connect surface nodes. The average number of connected surface nodes per air node, $\langle K \rangle / N$, can approach this upper bound either by the optimum choice of specific fixed locations for all surface nodes or by simply increasing the number of surface nodes underneath each aircraft, S^i, for any or all i. Increasing S^i enough to approach this bound, however, may cause low average surface-to-air connection availability, $\langle A_f \rangle$.

One important benchmark for a range extension network is the ability to maintain 100% availability for all connections. For arbitrarily located surface nodes (i.e., their location is unknown and unrestricted except to be on the earth's surface and within range of a given aircraft), a theoretical upper bound on the number of surface users per aircraft that can be supported with a guarantee of 100% available surface-to-air links can be written as a function of air topology and antenna FoV parameters as follows:

$$S^i \leq \left(\lfloor \frac{2\gamma}{\sigma} \rfloor + 1 \right) \frac{n_a}{n_s} - d^i_{air} \qquad (\text{ valid for } \gamma \leq 180^o[1 - 1/n_s] \,). \tag{3}$$

where $\lfloor x \rfloor$ denotes the greatest integer less than or equal to x, and where we assume that d^i_{air} is not large enough for the bound to be negative. This equation derives from the fact that there is a non-zero probability that all d^i_{air} connections and all S^i connections may fall into non-overlapping region of a single sector (Fig. 3) where there are only n_a/n_s beams available when γ is small.[4] If γ is large enough so that adjacent sectors have complete overlap (which is unlikely in practice), then any point in azimuth space will be covered by integer multiples of n_a/n_s beams

[4]If the air topology is designed so that all d^i_{air} nodes can never fall into a single sector, then d^i_{air} should be replaced in Eqn. 3 with $d^i_{sectors}$, the maximum number of air nodes that can fall within $\lfloor 2\gamma/\sigma \rfloor + 1$ sectors at any point during the aircraft orbit.

as indicated by the equation. The upper bound on the number of connected surface nodes in Eqn. (2) can be attained with guaranteed 100% connection availability for arbitrarily located surface nodes only when $\gamma = 180^o[1 - 1/n_s]$.

The total number of antenna beams per aircraft, n_a, will generally be severely restricted in aircraft pod designs due to size, weight, and power limitations of aircraft systems. It is important to maximize the number of user connections that can be obtained from a small number of beams for directional range extension applications. Fig. 7 illustrates the relationship between the number of antenna beams per pod, n_a, necessary to guarantee that S^i arbitrarily located surface nodes can be supported with a guarantee of $\langle A_f \rangle = 1$.

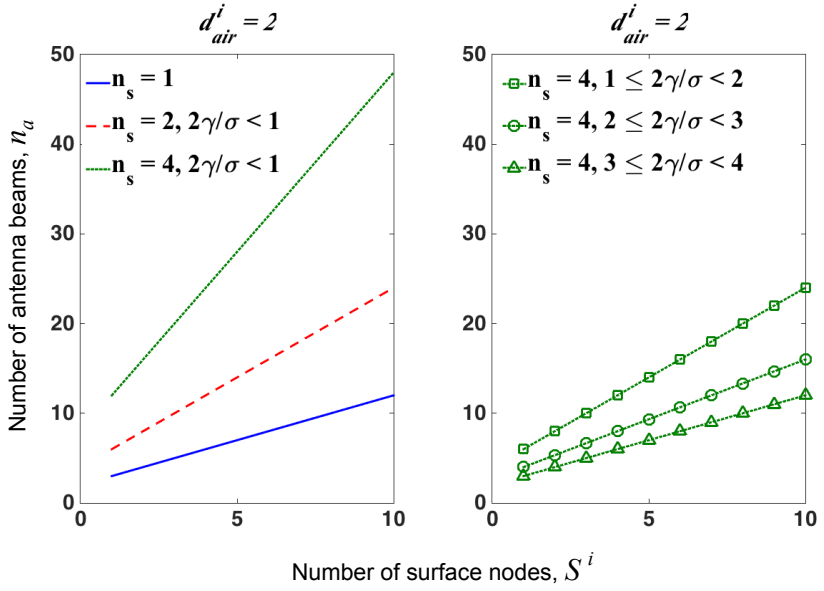

Fig. 7. Minimum number of antenna beams, n_a, required to guarantee $\langle A_f \rangle = 1$

The figure shows data for 1, 2, and 4 sector antennas. The left hand plot shows that for low amounts of FoV overlap between sectors (i.e., $2\gamma/\sigma < 1$), increasing the number of sectors dramatically increases the number of beams required to guarantee 100% surface-to-air connection availability. The right hand plot shows that increasing the FoV overlap, γ, between the sectors can ameliorate this problem, but the overlap must be quite large for substantial improvements. For example, for a 4-sector design to require as few antenna beams as a 2-sector design for $\langle A_f \rangle = 1$, the overlap must be $2\gamma/\sigma \geq 1$. While single sector antenna designs clearly offer the maximum theoretical surface user connections at 100% availability for the minimum number of beams, they may be difficult to implement in low size, weight, and power packages needed for

aircraft applications. Two-sector designs are likely to be more feasible in certain applications, and are examined as an important special case in the next subsection.

C. Two-Sector Antennas with Low Degree Air Topologies

In addition to showing the advantages of using a small number of antenna sectors, the results in Section IV-B also imply that the degree of the nodes in the air topology should be limited to maximize the interconnectedness of surface nodes and their connection availability. Ring topologies ($d^i_{air} = 2$ for all air nodes) or string topologies ($d^i_{air} = 2$ for all nodes except the ones on the ends of the string, where $d^i_{air} = 1$) are the most likely ways to form low degree connected air topologies. With the restriction of $d^i_{air} \leq 2$, the value of $\langle K \rangle / N$ can be written as a closed form equation for randomly and uniformly distributed surface node locations. Reference [15] derived this equation for the special case of $n_s = 2$, $S^i = S^j \ \forall i, j$, $\gamma = 0$ and $\delta = 0$. This subsection extends the derivation to arbitrary S^i and arbitrary values of γ and δ.

We assume that the local surface nodes served by a given aircraft lie within some range, R_{local}, of the centroid of the aircraft's flight path. For any given aircraft orientation, the antenna FoVs for each of the two sectors will map to three coverage areas on the surface of the earth: one area that is visible only to antennas on one end of the pod (pod "North"), another area that is visible only to antennas on pod "South", and an area that is visible to both antenna sectors simultaneously, as shown in Fig. 6b. While the boundaries between these sectors will depend in practice on the physical shape and configuration of the pod and antenna structures, we assume here that the physical blockages in both azimuth and elevation are caused by the pod structure with straight edges.[5] (Wing blockages are neglected in this model; they generally cause only short-duration blockages in near-circular flight paths.)

Fig. 8 shows the FoV layouts for conceptual ring and string topologies. The equation for $\langle K \rangle / N$ can be derived by considering each single air node in isolation. Using approximation 1) from Section III-B, the locations of other air and surface nodes relative to node i simply rotate in the azimuth plane of node i. A 360^o rotation corresponds to one complete circuit of a closed flight path, which has duration T^i. For a given node i, define time t_0 such that one of the neighbor air nodes (the only one in the case of a string end node) is positioned directly at the

[5]Straight edges are not likely in a real pod design for aerodynamic reasons, but are not too far different from what might be used in practice. They also make the approximate analysis tractable by causing the boundaries between FoV regions to be constant values of azimuth and elevation.

nose of the pod, and such that the other neighbor node (if any) is at an azimuth angle β_2^i such that $0 \leq \beta_2^i \leq 180^o$, as illustrated in Fig. 8. At time t_0, surface nodes may be located at azimuth angles that are either known and specified, or are unknown and assumed random. The remainder of this subsection derives closed form equations for the case of randomly located surface nodes. Section IV-D presents an algorithm for exact calculation of $\langle K \rangle / N$ for the cases of known (fixed) surface locations as well as the case of mixed known, fixed locations and random ones.

This analysis assumes that surface nodes of unknown location are equally likely to be at any location within a disc of radius R_{local} of the centroid of the aircraft flight path. Thus the locations of S^i surface nodes at time t_0 among the three FoV regions have a multinomial probability distribution with parameters $N_{multinomial} = S^i$, and

$$\begin{aligned} p_N &= p_S = \frac{1 - p_{NS}}{2} \\ p_{NS} &= \frac{\gamma}{90} + \frac{2A^2 tan^2\delta}{\pi R^2 tan\gamma} \quad \text{if } tan\delta \leq \frac{Rsin\gamma}{A} \\ &= 1 - \frac{\theta}{180} + \frac{sin\theta}{\pi} \quad \text{if } tan\delta \geq \frac{Rsin\gamma}{A} \end{aligned} \tag{4}$$

where $\theta = 2cos^{-1}(Atan\delta/R)$. Variables p_N, p_S, and p_{NS} are the probabilities of a node being in each of the three FoV regions – North only, South only, and North and South – respectively. A, R, and δ are as shown in Fig. 6, and all angles are in degrees.

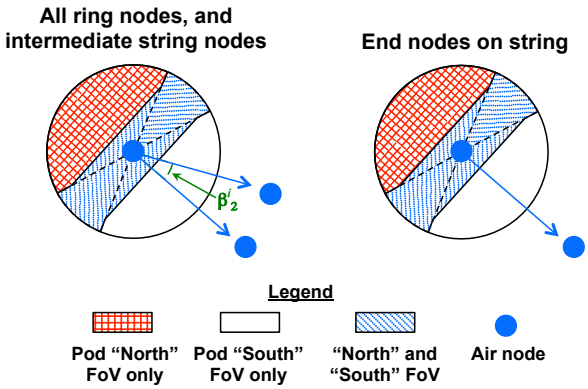

Fig. 8. Node locations from air node i for ring or string topologies

The number of surface nodes that can be supported at time t_0 can then be calculated as follows. The d_{air}^i air backbone connections are assumed to be given higher priority, thus reducing the number of antennas available to the surface nodes. The remote air node locations at $t = t_0$ are assumed known and are set at locations at pod "North" and pod North plus β_2^i, as described

above and shown in Fig. 8. $\langle K \rangle / N$ can be found by averaging the surface node locations over the multinomial distribution, and averaging both surface and remote air node locations over one 360^o rotation of node i's azimuth. However, the equations for the total number of connections unfortunately depend on the relative values of γ and β_2^i, complicating the derivation. The details of the derivation for $\langle K \rangle / N$ and the resulting Eqn. (A.7), are given in the Appendix A. Eqn. (1) gives the value of A_f as a function of $\langle K \rangle / N$.

The first observation we may make based on Eqns. (1) and (A.7) is that the elevation angle overlap parameter, δ, makes little difference in practical scenarios. Fig. 9 shows the contribution of δ to the FoV overlap region for a typical scenario where an aircraft is flying at 35,000 ft. and is serving local users within a 100 nautical mile radius. Especially when there is any significant overlap in the azimuth FoV, the effect of δ on the probability of a user being in the FoV overlap region is very small unless the overlap is quite large – tens of degrees, which is unlikely in practical designs. In the remainder of this paper, we shall neglect the effect of elevation overlap and assume $\delta = 0$.

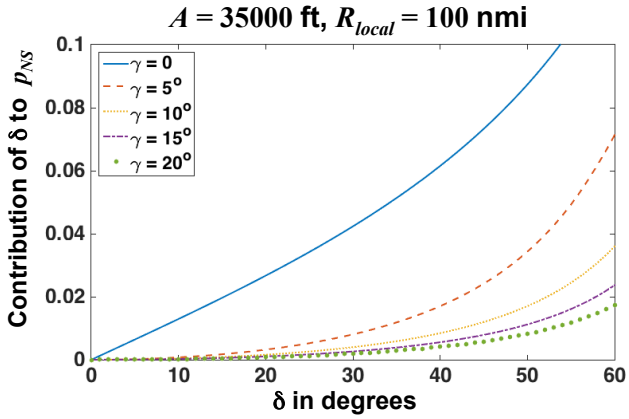

Fig. 9. Effect of the elevation angle overlap parameter δ at 35,000 ft altitude and 100 nmi local service area

In contrast, the azimuthal overlap, γ, can make a significant difference in some cases. Fig. 11 shows some sample results of these calculations for an arbitrarily selected regular air topology, illustrated in Fig. 10 with $N = 4$ air nodes, $\beta_2^i = 90^o$ for all air nodes, and $n_a = 6$ divided into two sectors. Fig. 11a shows the trade-off between $\langle K \rangle / N$ and A_f for increasing S^i, and also shows how the azimuthal FoV overlap γ makes a significant difference for a certain range of S^i, typically in the vicinity of $S^i = n_a - d_{air}^i$. Fig. 11b shows the effect of increasing γ for $S^i = 4$. Note how the connection availability increases from under 80% with no FoV overlap

to well over 90% for a modest 20^o to 30^o overlap. (See [15] for examples showing the relative performance of ring and string topologies in several example topologies for $\gamma = 0$.)

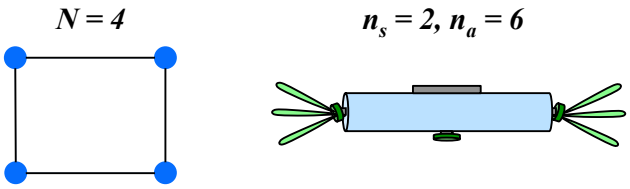

Fig. 10. Example scenario with four-node regular air topology and $n_a = 6$ antenna beams

D. Higher Degree Air Topologies and More than Two Antenna Sectors

For scenarios with fixed surface node locations (or a mix of fixed and random locations), $d^i_{air} > 2$, and/or $n_s > 2$, a closed form solution for $\langle K \rangle / N$ becomes very complicated and difficult to obtain. However, a simple heuristic can be used to calculate this quantity in any of these cases. The key insight to this heuristic is that at any time, t, if the azimuth angles to all surface and air nodes in transmission range of an air node i are known, the total number of nodes that can be connected to node i can be calculated exactly via a graph matching algorithm, and will remain constant as the aircraft flies around its orbit until one of these nodes crosses a FoV boundary between sectors. Thus, the durations between boundary crossings can be calculated, the number of connected nodes between each boundary crossing being constant, and the average number of connected nodes over one orbit period T^i can be directly obtained from these durations and connectivity calculations. Random node locations can be added to this procedure by using Monte Carlo techniques to randomly add nodes at specific locations for each trial and then running the algorithm for known node locations for each trial.

As in Section IV-C, we proceed by considering each air node in isolation. For each air node i, we define a set of angular boundaries, $\{B_k\}$, $0 \leq k \leq 2n_s - 1$, sorted in increasing order, that represent the azimuth angles of coverage region boundaries. Fig. 12a illustrates the eight coverage regions for $n_s = 4$ (each light or dark shaded region is one coverage region). We assume for simplicity of description that the region bounded by B_0 and B_1 is an overlap region (one of the dark shaded regions in Fig. 3), rather than a non-overlap region, though this assumption is not strictly necessary. Given a topology with fixed node locations, we represent the azimuth angles at time t of all surface and air nodes by the set of angles $\{\alpha_j(t)\}$, where $1 \leq j \leq S^i + d^i_{air}$.

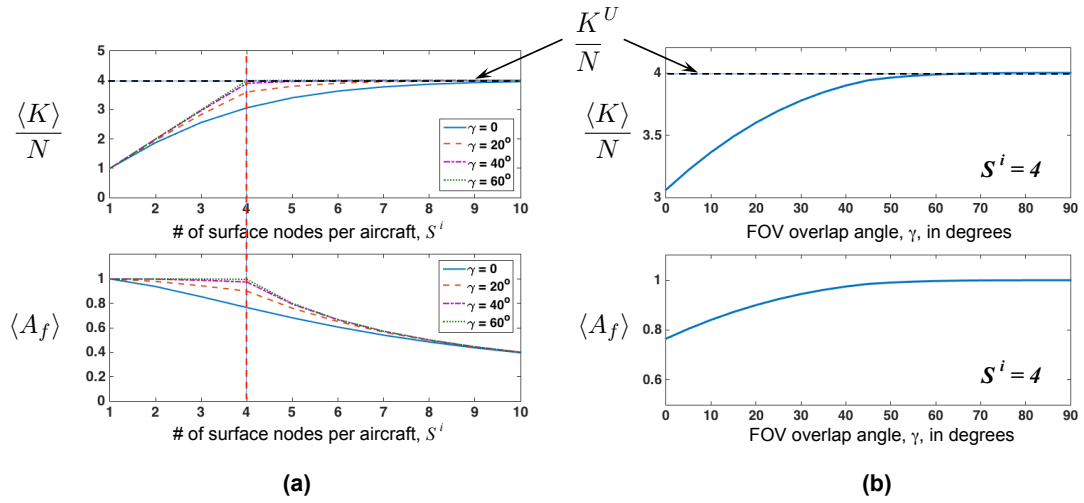

Fig. 11. Expected number of surface nodes connected and connection availability for regular four-node air topology: a) vs. number of surface nodes, b) vs. FoV overlap γ for $S^i = 4$

Let t_1 be the time when an arbitrary node azimuth satisfies $\alpha_j(t_1) = B_0$, that is, a time when one of the local or remote nodes is exactly on the coverage region boundary with the smallest azimuth value. Let $\alpha_j^B(t_1) = (\alpha_j(t_1) - B_0) \bmod 360^o$ be the node azimuth angles relative to the boundary B_0, and sort $\alpha_j^B(t_1)$ in increasing order. Table II summarizes these definitions.

TABLE II

PARAMETERS FOR ALGORITHM TO CALCULATE $\langle K \rangle$

$\{B_k\}$	Set of FoV boundaries between antenna sectors
$\{\alpha_j(t)\}$	Set of azimuth values at node i for surface and air nodes at time t
t_1	Time at which $\alpha_j = B_0$ for some node j
$\{\alpha_j^B(t_1)\}$	Set of node azimuth values relative to B_0 and sorted in increasing order
m	Increment counter for algorithm
T_m	Duration between boundary crossings for increment m
K_m^i	Number of connected surface nodes at node i during increment m
$K_m^{i,tot}$	Number of connected surface and air nodes at node i during increment m
$\langle K^i \rangle$	Average number of connected surface nodes at node i

We can calculate the average number of nodes (including both surface and air nodes) connected to node i over the interval $t_1 \le t \le t_1 + T^i$ by the following procedure. There are $2n_s[S^i + d_{air}^i]$ boundary crossings during the period $t_1 \le t \le T^i + t_1$. Assuming that the aircraft fly at constant

velocities such that $\alpha_j^B(t)$ increase in linear proportion to t, the duration between each pair of boundary crossings, T_m, can be calculated by finding the minimum angular difference between each $\alpha_j^B(t)$ and each boundary B_k and dividing this difference by an (arbitrary) assumed rate of speed of the aircraft. Once T_m is calculated for all $2n_s(S^i + d_{air}^i)$ boundary crossings, we need only calculate the number of connected surface nodes, K_m, during each interval m.

We can calculate the *total* number of connected nodes at node i during the m^{th} interval, $K_m^{i,tot}$, by setting up a graph matching problem and using an augmenting path algorithm to find a maximum cardinality matching [19]. At any given time, t, between t_1 and $t_1 + T^i$, we can construct a bipartite graph $G = (U, V, E)$ representing the remote nodes with azimuths $\{\alpha_j^B(t)\}$ and their visibilities from the antenna beams at node i. A bipartition (U, V) is constructed where the vertices in U represent the set of nodes in range of node i, and the vertices in V represent the set of antenna beams on node i. $G = (U, V, E)$ is then formed by placing edges E between each vertex in U and vertices in V that represent the antenna beams having a clear FoV to the surface or air node represented by the vertex in U. Fig 12b shows an example of such a graph for the example case in Fig. 12a, with $n_a = 8$ and $n_s = 4$, producing two beams per sector. The maximum cardinality matching gives $K_m^{i,tot}$, the number of nodes that can be connected to air node i during the m^{th} time increment. We then have $K_m^i = K_m^{i,tot} - d_{air}^i$, and $\langle K^i \rangle = \sum_m T_m K_m^i / T^i$. Algorithm 1, which can be extended to any sectorized antenna structure that can be represented by a set of boundaries with alternating overlap and non-overlap regions, formalizes this calculation.

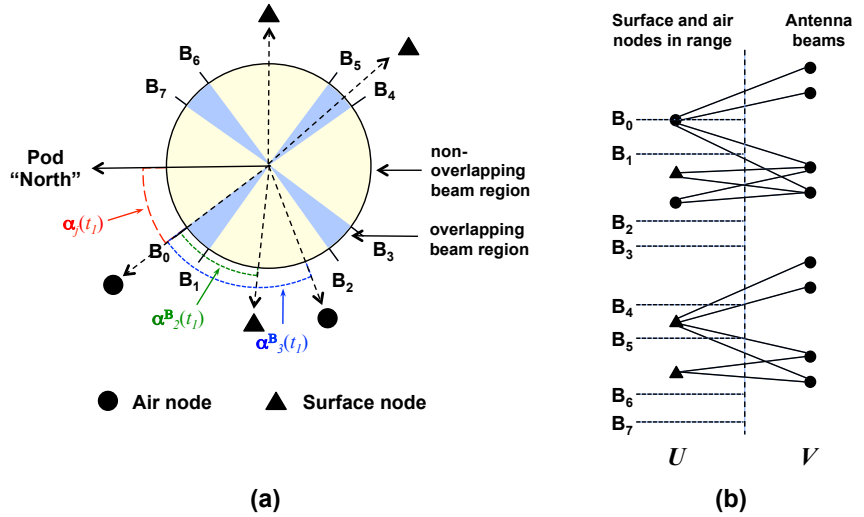

Fig. 12. Example node geometry for $n_s = 4$: (a) azimuth locations; (b) equivalent bipartite graph for $n_a/n_s = 2$

Algorithm 1 Calculate $\langle K \rangle$ for Fixed Surface Nodes

$t = t_1$ ▷ Initial value of t
for $i = 1$ to N **do** ▷ For each air node
  Initialize index value $m = 1$
  while $t < t_1 + T^i$ **do**
    Form bipartite graph $G = (U, V, E)$ representing node visibilities
      U = Set of surface and air nodes in range of node i
      V = Set of antenna beams at node i
      E = Connections between antenna beams and visible nodes
    $K_m^{i,tot}$ = maximum cardinality matching on G ▷ Augmenting Path Algorithm
    Calculate T_m ▷ Time until next boundary crossing
    $t = t_1 + T_m$
    $m = m + 1$
  end while
  $K_m^i = K_m^{i,tot} - d_{air}^i$
  $\langle K^i \rangle = (\sum_m K_m^i T_m)/T^i$
end for
return $\langle K \rangle = \sum_{i=1}^{N} \langle K^i \rangle$

Fig. 13 shows $\langle K \rangle / N$ and A_f for the regular four-air-node topology of Fig. 10 with random surface node locations, and with $n_a = 8$ total antenna beams, divided evenly among one, two, and four sectors, and for three different values of azimuthal overlap γ. For a given value of total azimuth overlap, $2\gamma n_s$, the performance is uniformly better for smaller n_s. The best performance is given by the one-sector system, which attains the performance bound of eqn. (2) for $S^i = 6$ surface nodes with 100% availability, and maintains both higher connectedness and availability for any value of S^i. The two-sector model with $\gamma = 40$ nearly equals this performance, however, and the 4-sector model with $\gamma = 20$ outperforms the 2-sector model with $\gamma = 0$.

Fig. 14 shows another set of example results for the two realistic topologies shown in Fig. 5. These results assume $n_s = 2$ sectors, $n_a = 4$ total antennas. The topologies have $S^i = 2$ for two of the relay aircraft and $S^i = 1$ for the other two, and $d_{air}^i = 2$ for two of the air nodes and $d_{air}^i = 1$ for the other two. The solid curves show availability results for all surface nodes fixed in the locations shown in the figures, and the dashed curves show results for the two land-based surface

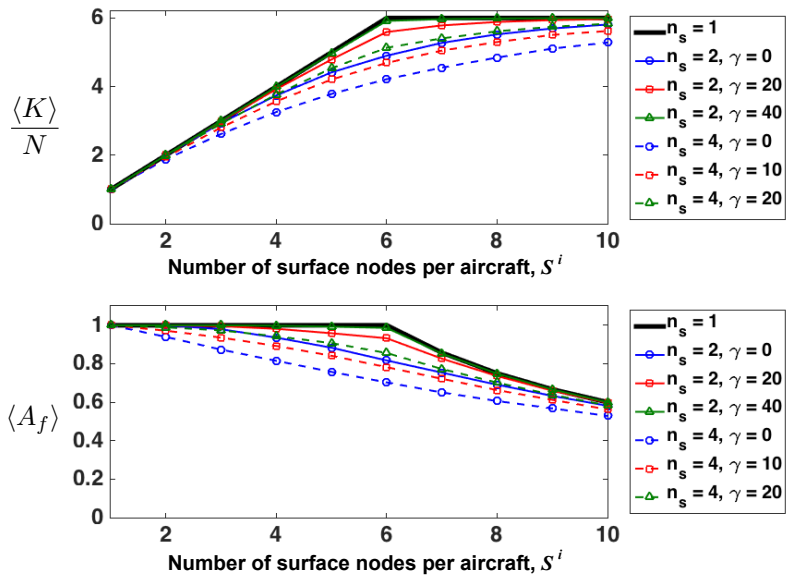

Fig. 13. Example results comparing performance for $N = 4$, $n_a = 8$, for varying n_s and γ

nodes being fixed while the sea-based nodes are assumed randomly located. The results both illustrate the performance comparisons that can be obtained for any combination of the parameters modeled in this paper, as well as showing the benefits of even a marginal amount of azimuthal overlap for a two-sector system. The topology T1 has an overall lower air topology degree, and thus has more available antenna beams to support surface nodes at higher availabilities. Topology T2 is more connected in the air domain with resultant lower average availability of surface node connections, but even a 20^o overlap can increase the average availability from under 80% to well over 90%, which can be quite significant in tactical range extension situations.

Table III compares the performance of 2-sector antennas with no sector overlap ($\gamma = 0$) and with 4 and 6 beams for the same two topologies and mix of random and fixed surface node locations as the previous figure. Not surprisingly, there is a notable improvement in both connectedness and availability from adding two extra antenna beams, and all the surface nodes can be serviced with 100% connection availability for topology T1 with $n_a = 6$ for either completely fixed surface nodes or mixed random and fixed locations.

V. Discussion

It is clear that the number of sectors in an antenna design for the type of range extension scenario described in this paper should be a minimum. Theoretically, it would be best to be

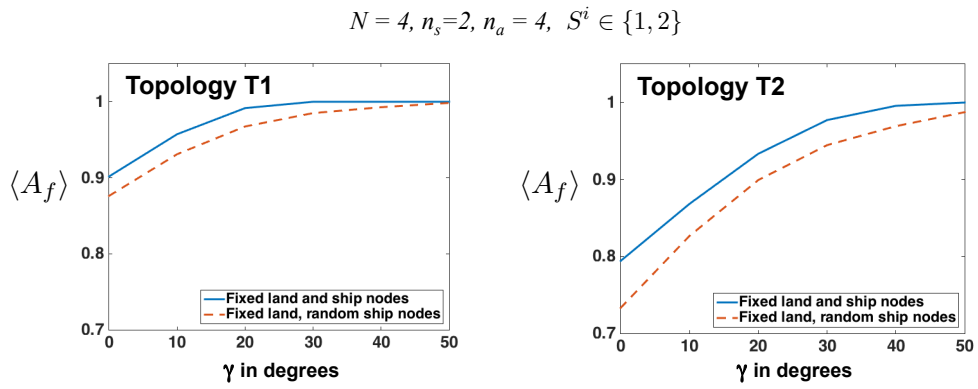

Fig. 14. Example results comparing performance the two topologies of Fig. 5 and showing the effects of azimuthal overlap γ

TABLE III

COMPARISON OF 2-SECTOR ANTENNAS WITH 4 AND 6 BEAMS FOR THE EXAMPLE TOPOLOGIES OF FIG. 5

	$n_a = 4$		$n_a = 6$	
	Topology T1	Topology T2	Topology T1	Topology T2
	Fixed land and ship locations			
$\langle K \rangle / N$	1.35	1.19	1.5	1.46
$\langle A_f \rangle$	0.9	0.79	1	0.98
	Fixed land, random ship locations			
$\langle K \rangle / N$	1.31	1.10	1.5	1.48
$\langle A_f \rangle$	0.88	0.73	1	0.99

able to cover all 360^o of aircraft azimuth space with a single set of n_a directional antenna beams. This type of design may possibly be accomplished with multi-element phased arrays where several multi-element arrays are distributed around the sides of the pod and centrally processed by digital beamforming techniques. The major practical limitations of this technique are probably the substantial processing power required to form multiple beams in real time and the requirement to divide transmit power among multiple beams. In the near term this may not be feasible with the highly limited size, weight, and power that are available from typical candidates for relay aircraft. However, in the longer term, this type of design may have the best potential for supporting high-availability aerial range extension. In the near term, 2-sector designs may be more feasible, and may even be implemented with mechanically steered directional antennas. Reference [15] summarizes some of the other technologies that require further development to

improve the performance of this type of system.

VI. Summary and Conclusions

This paper has presented an approximate analysis of the average interconnectedness, $\langle K \rangle$, and link availabilities, $\langle A_f \rangle$, of a range extension network using aerial relay nodes with highly directional antenna beams. The antennas are assumed to have substantial field-of-view (FoV) restrictions that are caused by structural blockages. The analysis models various antenna design parameters (e.g., number of sectors, number of beams) and network topology parameters (e.g., numbers, locations, and connectivity of air and surface nodes). The equations and algorithms presented allow generalized modeling of performance trade-offs for various combinations and choices of these design parameters.

A number of example results have been presented, which show that:

- Both interconnectedness and availability are maximized by using the smallest number of sectors possible to cover the entire 360^o of azimuth in the aircraft-based antenna designs;
- Aircraft antenna designs using more than one sector to cover the entire 360^o in azimuth make interconnectedness and availability dependent on the physical geometry of network topology;
- The azimuthal overlap between sector FoVs has a significant effect on performance, while the elevation FoV overlap generally does not;
- There is a trade-off between the number of surface nodes that can be supported by each aircraft and the average availability of the surface-to-air connections for these nodes.

There are a number of opportunities for future work in this area. While this paper implies that low degree air topologies maximize the connectedness and availability of surface node connections, algorithms for managing these topologies still require a great deal of development, especially if the scale of the network is to extend to more than just a few air relay nodes [2][3][15]. Frequency management of both air-to-air and air-to-surface links is also a difficult issue requiring further research, especially given the highly constrained state of spectrum availability worldwide. The modeling in this paper could also be extended to cover effects such as aircraft wing blockages, especially of air-to-air links. Finally, the development of antenna technologies to enable the types of multiple beam pointing capabilities described in this paper with minimal size, weight, and power, is of great importance and requires many implementation issues to be addressed.

APPENDIX A

This appendix derives the equations for $\langle K \rangle / N$ for the special case of $n_s = 2$, $d^i_{air} \leq 2 \ \forall i$, and randomly located surface nodes within a range R_{local} of the centroid of the aircraft's orbit.

As described in Section IV-C, $\langle K \rangle / N$ can be derived by taking the expectation of the number of connected surface nodes over a multinomial distribution of surface node locations. The analysis must be broken up into six different cases – each corresponding to a particular range of the relationship between β^i_2 and γ – and four different air-to-air FoV states. The six cases are shown in Fig. 15.

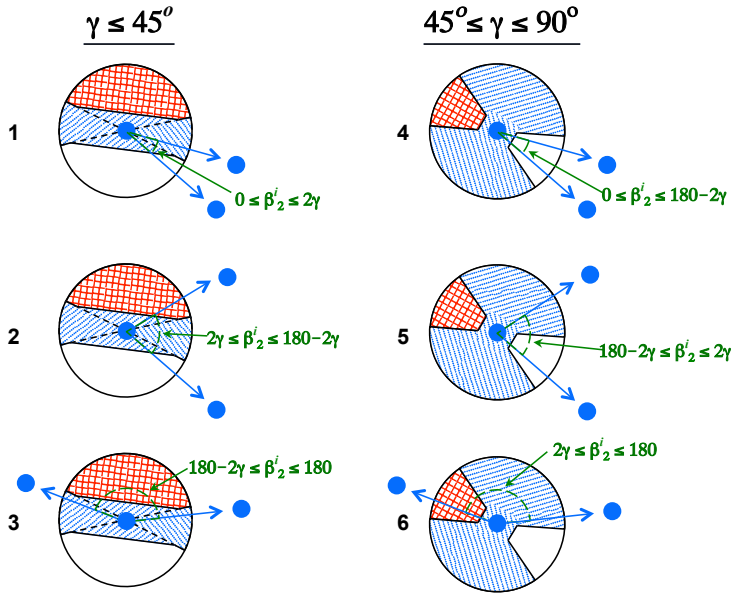

Fig. 15. Six different cases of relationships between γ and β^i_2

In each case, a subset of four air-to-air FoV states is possible when $d^i_{air} = 2$. The four states are:

- FoV State 1: Both remote air nodes are visible from the same single sector only;
- FoV State 2: Each remote air node is visible from a different sector only;
- FoV State 3: One remote air node is visible only from a given sector but the other is visible from either sector;
- FoV State 4: Both remote air nodes are visible from either sector.

Table IV shows which FoV states are possible for each of the six cases of Fig. 15.

We define the number of surface nodes connected to node i in State l at time t_0 as K_{state_l} and the number of connected surface and air nodes at node i at t_0 as $K^{tot}_{state_l} = K_{state_l} + d^i_{air}$. In

TABLE IV

RELATION OF FOUR FOV STATES TO SIX CASES OF γ AND β_2^i

	FoV State 1	FoV State 2	FoV State 3	FoV State 4
Case 1	X		X	X
Case 2	X	X	X	
Case 3		X	X	X
Case 4	X		X	X
Case 5			X	X
Case 6		X	X	X

each of the four FoV states, the total number of connected nodes, K_l^{tot}, is given by the following equations:

$$K_{state_1}^{tot} = min\left\{\left[min\left[\frac{n}{2}, (d_{air}^i + j)\right] + min\left[\frac{n}{2}, k\right] + (S^i - j - k)\right], \left[n\right]\right\} \tag{A.1}$$

$$K_{state_2}^{tot} = min\left\{\left[min\left[\frac{n}{2}, (d_{air}^i - 1 + j)\right] + min\left[\frac{n}{2}, (d_{air}^i - 1 + k)\right] + (S^i - j - k)\right], \left[n\right]\right\} \tag{A.2}$$

$$K_{state_3}^{tot} = min\left\{\left[min\left[\frac{n}{2}, (d_{air}^i - 1 + j)\right] + min\left[\frac{n}{2}, k\right] + (S^i + d_{air}^i - 1 - j - k)\right], \left[n\right]\right\} \tag{A.3}$$

$$K_{state_4}^{tot} = min\left\{\left[min\left[\frac{n}{2}, j\right] + min\left[\frac{n}{2}, k\right] + (S^i + d_a^i - j - k)\right], \left[n\right]\right\} \tag{A.4}$$

where j, k, and $(S^i - j - k)$ are the numbers of nodes visible from pod North, pod South, and both sectors, respectively.

At time $t = t_0$, the remote air node locations will be in one of the four FoV states, and we can calculate the expected value of the appropriate K_{state_l} taken over the multinomial distribution, which can be written as

$$\langle K \rangle = \sum_{j=0}^{S^i} \sum_{k=0}^{S^i - j} C_{jk} K_{state_l} - d_{air}^i \tag{A.5}$$

where

$$C_{jk} = \frac{S^i! p_N^j p_S^k p_{NS}^{S^i - j - k}}{j!k!(S^i - j - k)!}$$

are the multinomial coefficients with the probabilities p_N, p_S, and p_{NS} as defined in Eqn. (4).

To calculate the average $\langle K \rangle / N$ over an entire aircraft orbit period T^i for all air nodes, we must average this quantity over one orbit duration T^i for each node i. This becomes complicated, since as each aircraft flies through its orbit, the FoV state changes, and the changes are dependent on which of the six cases of relationship between γ and β_2^i holds. For Case 1 ($0 \leq \beta_2^i \leq 2\gamma$), the average number of air nodes connected to node i over one orbit period is given by

$$\langle K \rangle = \sum_{j=0}^{S^i} \sum_{k=0}^{S^i-j} C_{jk} \left[\left(1 - \frac{\beta_2^i + 2\gamma}{180} \right) K_{state_1}^{tot} + \frac{\beta_2^i}{90} K_{state_3}^{tot} + \frac{2\gamma - \beta_2^i}{90} K_{state_4}^{tot} \right] - d_{air}^i \tag{A.6}$$

The equations for all six cases can be combined into a single equation, averaged over all N air nodes in the topology, and normalized to N, yielding:

$$\frac{\langle K \rangle}{N} = \frac{1}{N} \sum_{i=1}^{N} \left\{ \left[\sum_{j=0}^{S^i} \sum_{k=0}^{S^i-j} C_{jk} \left(A_1 K_{state_1}^{tot} + A_2 K_{state_2}^{tot} + A_3 K_{state_3}^{tot} + A_4 K_{state_4}^{tot} \right) \right] - d_{air}^i \right\} \tag{A.7}$$

where

$$\begin{aligned} A_1 &= \frac{max[(180 - \beta_2^i - 2\gamma), 0]}{180} \\ A_2 &= \frac{max[(\beta_2^i - 2\gamma), 0]}{180} \\ A_3 &= \frac{min[2\gamma, \beta_2^i, (180 - \beta_2^i), (180 - 2\gamma)]}{90} \\ A_4 &= \frac{max[(2\gamma - \beta_2^i), (2\gamma + \beta_2^i - 180), (4\gamma - 180), 0]}{180} \end{aligned} \tag{A.8}$$

A check on the correctness of this equation is that it can be shown to reduce to the following equation, which was derived in [15], for the special case of $\gamma = 0$ and $\delta = 0$ (where the surface nodes are distributed binomially instead of multinomially):

$$\begin{aligned} \frac{\langle K \rangle}{N} = \frac{1}{N} \sum_{i=1}^{N} \Bigg\{ & \frac{\beta_2^i}{180} \left[\sum_{j=0}^{S^i} \frac{1}{2^{S^i}} \binom{S^i}{j} \left(min[\frac{n_a}{2}, (d_{air}^i - 1 + j)] + min[\frac{n_a}{2}, (S^i - j + 1)] \right) \right] \\ & + \left(1 - \frac{\beta_2^i}{180} \right) \left[\sum_{j=0}^{S^i} \frac{1}{2^{S^i}} \binom{S^i}{j} \times \left(min[\frac{n_a}{2}, j] + min[\frac{n_a}{2}, (S^i - j + d_{air}^i)] \right) \right] - d_{air}^i \Bigg\} \end{aligned} \tag{A.9}$$

APPENDIX B

This appendix shows that the approximation of constant compass directions during an entire aircraft orbit are quite good for circular orbits of any radius. Fig. 16 shows a relay aircraft flying a circular orbit of radius r_{orb} about some center point. Let R be the distance from this center to another node, either a remote air node or a local surface node. As the aircraft flies around its orbit, let $\phi(t)$ be the angular difference between its position at time t_0 and at time t referenced to the center point, and let α_{t_0} be the angular difference between a vector from the center point

to the aircraft's position at t_0 and a vector to the remote air node. The true azimuth of the remote node relative to node i will differ from the azimuth produced by the approximation that the aircraft's orbit has radius approaching zero. The difference can be solved for using standard formulas of oblique trigonometry. Table V shows the azimuth errors for the entire orbit period, making use of the definition

$$\Theta(t) = cos^{-1}\left(\frac{2r_{orb}^2 - 2Rr_{orb}cos(\alpha_{t_0} - \phi(t))}{2r_{orb}[R^2 + r_{orb}^2 - 2Rr_{orb}cos(\alpha_{t_0} - \phi(t))]^{\frac{1}{2}}}\right) \tag{B.1}$$

TABLE V

APPROXIMATED VS. TRUE AZIMUTH FOR $r_{orb} > 0$

	$0^o \le \alpha_{t_0} - \phi(t) \le 180$	$-360 \le \alpha_{t_0} - \phi(t) \le -180$	$180 \le \alpha_{t_0} - \phi(t) \le 360$	$-90 \le \alpha_{t_0} - \phi(t) \le 0$
$Az_{app.}$	$\alpha_{t_0} - \phi(t)$	$360 + \alpha_{t_0} - \phi(t)$	$\alpha_{t_0} - \phi(t)$	$360 + \alpha_{t_0} - \phi(t)$
Az_{true}	$180 - \Theta$	$180 - \Theta$	$180 + \Theta$	$180 + \Theta$
Az_{error}	$180 - \Theta - (\alpha_{t_0} - \phi(t)$	$-(\alpha_{t_0} - \phi(t)) - \Theta - 180$	$180 + \Theta - (\alpha_{t_0} - \phi(t))$	$\Theta - 180 - (\alpha_{t_0} - \phi(t))$

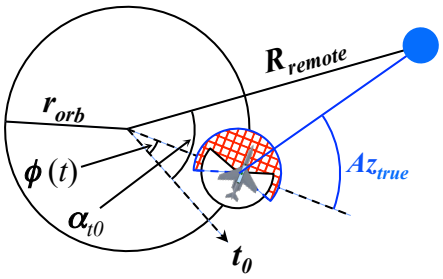

Fig. 16. Parameters for circular aircraft orbit with finite radius

Fig. 17 shows azimuth errors as a function of time for three different values of R: the first one typical of a remote air node, the second one slightly greater than r_{orb} and the third one slightly less than r_{orb} (the second and third represent interesting cases for local surface node locations). The error for a typical remote air node is quite small, but the errors for nearby nodes are very large. However, in all cases the errors are symmetric around a zero crossing somewhere in the orbit (the value of $\phi(t)$ for the zero crossing depends on the value of α_{t_0}). Because the errors are symmetric about zero, they will cancel out when averaged over an entire orbit period T^i, and the average quantities calculated in this paper will be exact as long as they are averaged

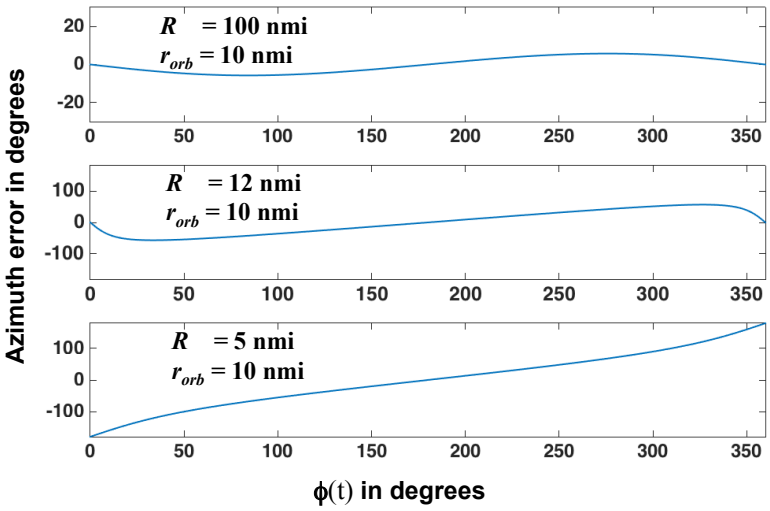

Fig. 17. Azimuth errors over one orbit period for three cases of R and for $\alpha_{t_0} = 0$. (Note that the top plot Y-axis is different in scale from the bottom two.)

over any integer multiple of T^i. However, non-circular orbits may cause values of $\langle K \rangle$ and A_f to deviate from their true values.

ACKNOWLEDGEMENTS

The authors would like to thank Terrance Gibbons of MIT Lincoln Laboratory's Tactical Networks Group for supplying details of the example four-aircraft scenarios in Fig. 5.

REFERENCES

[1] D. Mehta, B. Ganguly, "The Effect of Platform Dynamics on Aerial Layer Network Performance", IEEE Milcom2014, Oct. 2014

[2] J. Wang. P. Deutsch, A. Coyle, T. Shake, B-N Cheng, "An Implementation of a Flexible Topology Management System for Aerial High Capacity Directional Networks", IEEE Milcom2015, Oct. 2015

[3] J. Wang, T. Shake, P. Deutsch, A. Coyle, B-N Cheng, "Topology Management Algorithms for Large-Scale Aerial High Capacity Directional Networks", accepted for IEEE Milcom2016, Nov. 2016

[4] C. Cirullo, R. Olsen, C. Meagher, R. Ferro. P. Crescini, L. Maguire, "Network Solutions for Employing COTS Radios in Multi-Sector Directional Architectures", IEEE Milcom2008, Nov. 2008

[5] C. Meagher, R. Olsen, C. Cirullo, R. Ferro, N. Stevens, J. Yu, "Directional Ad Hoc Networking Technology (DANTE) Performance at Sea", IEEE Milcom2011, Nov. 2011

[6] J. Litva and T. K. Lo, *Digital beamforming in wireless communications*, Artech House, Inc., 1996

[7] B. D. Van Veen and K. M. Buckley, "Beamforming: A versatile approach to spatial filtering?", IEEE assp magazine, vol. 5, no. 2, pp. 4?24, 1988

[8] P. Santi, "Topology Control in Wireless Ad Hoc and Sensor Networks", *ACM Computing Surveys*, Vol. 37, No. 2, June 2005

[9] O. Bazan, M. Jaseemuddin, “A Survey On MAC Protocols for Wireless Adhoc Networks with Beamforming Antennas", *IEEE Communication Surveys and Tutorials*, Vol. 14, No. 2, Second Quarter 2012

[10] D. Van Hook, M. Yeager, J. Laird, “Automated Topology Control for Wideband Directional Links in Airborne Military Networks", IEEE Milcom2005, Oct. 2005

[11] P. Wang, B. Henz, “Antenna Assignment for JALN HCB", IEEE Milcom2015, Oct 2015

[12] J. Zhuang, M. Casey, S. Milner, S. Gabriel, G. Baecher, “Multi-Objective Optimization Techniques in Topology Control of Free Space Optical Networks", IEEE Milcom2004, Nov. 2004.

[13] A. Desai, S. Milner, “Autonomous Reconfiguration in free-Space Optical Sensor Networks", *IEEE Journal on Selected Areas in Communications*, Vol. 23, No. 8, Aug. 2005

[14] A. Kashyap, K. Lee, M. Kalantari, S. Khuller, M. Shayman, “Integrated topology control and routing in wireless optical mesh networks", *Computer Networks*, Vol 51, pp. 4237-4251, 2007

[15] T. Shake, “Topology Design for Directional Range Extension Networks with Antenna Blockage", submitted to IEEE WCNC 2017

[16] T. Stahlbuhk, B. Shrader, E. Modiano, “Topology Control for Wireless Networks with Highly-Directional Antennas", 14th International Symposium on Modeling and Optimization in Mobile, Ad Hoc, and Wireless Networks (WiOpt), May 2016

[17] T. Cormen, C. Leiserson, R. Rivest, and C. Stein, *Introduction to Algorithms (3rd ed.)*. MIT Press, 2009

[18] T. Bonald, L. Massoulié, “Impact of fairness of Internet performance", ACM SIGMETRICS 2001

[19] D. Jungnickel, *Graphs, Networks, and Algorithms*, Springer 1999

[20] M. Stoer, *Design of Survivable Networks*, Lecure Notes in Mathematics #1531, Springer-Verlag, 1991

[21] C. Colbourn, *The Combinatorics of Network Reliability*, Oxford University Press, 1987

[22] R. Freeman, *Fiber-Optic Systems for Telecommunications*, Wiley-Interscience, 2002. See Chapter 12.

[23] Cardwell, R. H., Monma, C. L., Wu, T. H., “Computer-aided Design Procedures for Survivable Fiber Optic Networks", *IEEE Journal on Selected Areas in Communications*, vol. 7, no. 8, October 1989

[24] T. Shake, B. Hazzard, D. Marquis, “Assessing Network Infrastructure Vulnerabilities to Physical Layer Attacks", 27th National Information Systems Security Conference, Oct. 1999